XLIII CILAMCE
21–25, November, 2022
FOZ DO IGUAÇU – PR – BRAZIL

A new dual boundary element formulation for cohesive crack propagation

Gustavo O. Daumas, Guilherme H. Teixeira, Rafael M. Lins, Sérgio G. F. Cordeiro, Francisco A. C. Monteiro

Laboratório de Modelagem Estrutural – LME, Instituto Tecnológico de Aeronáutica
Praça Marechal Eduardo Gomes,50, Vila das Acácias, 12.228-900, São José dos Campos/SP, Brasil
gustavo.daumas@ga.ita.br, guilherme.teixeira@ga.ita.br, mlins@ita.br, cordeiro@ita.br, facm@ita.br

Abstract. A cohesive dual boundary element formulation is presented for crack propagation analysis and a path-following method is proposed to solve the nonlinear system of equations by the direct control of one of the known degrees of freedom. The simple linear cohesive model is introduced into the algebraic boundary element equations by local stiffness matrices. According to the cohesive law, the stiffness coefficients decays as crack displacement discontinuities increases. The acting loads are divided into two groups: one in which the load is perfectly known and another in which only the direction is known. The magnitude (or load factor) of the latter is determined with respect to the equilibrium of the boundary fields (indirectly controlled) and an additional path-following constraint equation. The resulting non-linear system is solved using an incremental iterative scheme. For each iteration, the corrections to the boundary fields are obtained in a partitioned manner, in which the load factor is calculated independently using the direct control of the degree of freedom as the path-equation. The results show that the proposed approach can efficiently capture the equilibrium curves.

Keywords: dual boundary element method, cohesive model; path-following methods.

1 Introduction

Fractures have been a major engineering problem since the beginning of human development. It is of vital importance to know how the failure of materials occurs and thus work towards safety, saving materials and correctly designing each type of structure for its intended purpose. There are manly two ways to account for the influence of cracks within a structure: discrete cracks or continuous approaches. The continuous approaches, namely, continuum damage mechanics [1] and phase-field methods [2], results naturally in nonlinear problems. Within the discrete crack approaches, the physical non-linearities can appear both in the bulk material, as in the case of elastoplastic fracture mechanics [3], as well as in the crack surfaces itself, which is a common feature of cohesive models [4]. Cohesive models replace the fracture processes zone near the crack tip (zone where energy dissipation occurs due to physical nonlinearities) by a fictitious crack which its surfaces are subjected to cohesive stresses, written as a function displacement discontinuity. Thus, it is imposed to the model that the dissipated energy in the fictitious crack must be equal to the dissipated fracture energy in the process zone. The first cohesive model was proposed by [5] for the analysis of crack propagation in ductile materials. [6] extended the cohesive models for quasi brittle materials, in which the dissipated energy in the fracture process zone is meanly due to micro-cracking. Now a days, several physical consistent cohesive models, including potential and damage-based ones, can be found in the literature [4, 7].

The boundary element method is a numerical method that can solve solid mechanics boundary value problems with a smaller order of spatial discretization than other domain methods, namely, the finite element method. When applied to model a discrete crack, the overlapping crack surfaces will generate linear dependent equations into the algebraic system of equations, making its solution impossible. In this sense, the dual boundary element formulation [8-10] came to circumvent these limitations. The dual boundary element method is a collocation weighted residual method, in which for collocation points at one face of the crack imposes the

displacement integral equation and for the symmetric collocation point on the other crack face imposes the traction integral equation. Since these dual integral equations are linear independent, it is possible to solve the problem requiring the spatial discretization only at the boundary and crack surfaces. Other approaches to model discrete cracks using boundary element formulations include the displacement discontinuity method [11, 12], the sub-region technique [13, 14], the use of specialized fundamental solutions of solids containing cracks [15], the dipole formulation [16, 17] and Galerkin formulations [18].

Since both boundary displacements and tractions are field variables in boundary element method, cohesive modes can be introduced in the formulation in a more direct way. Aliabadi [19] presented for the first time a cohesive dual boundary formulation to address crack growth in concrete. It is worth mentioning that the introduction of the cohesive model into the boundary element formulation results in a nonlinear system of equations, which requires special techniques for its numerical resolution. Leonel and Venturini [20] presented a purely Newton-Raphson procedure, i.e., the tangent operator, to solve the nonlinear system of equations during the cohesive propagation analysis in quasi brittle materials. It was show that such an operator resulted in a small number of iterations for the convergence of the nonlinear analysis compared to previous approaches. Cordeiro and Leonel [21] applied the cohesive dual boundary formulation and the tangent operator technique for quasi brittle crack propagation analysis in anisotropic materials. Even though the tangent operator converges faster to the solution of the nonlinear equations, it presents some drawbacks in the presence of instabilities. Besides, in both works by Leonel and Venturini [20] and Cordeiro and Leonel [21], the sub-matrices involved in the calculation of the residue vector changes dimensions during the crack propagation, introducing difficulties in the implementation of more sophisticated cohesive models.

It is well-known in the literature that purely Newton-based approaches, such as the tangent operator, fails in obtaining the equilibrium trajectories in the face of instabilities such as the snapping effects [22]. Riks [23] proposed that snapping phenomena could be adequately addressed by complementing the equilibrium equations (residue equal to zero) with an auxiliary equation, namely, the path-equation. In that case, the path-equation represented a restriction on the path size to be followed along the equilibrium curve for a given loading step. This way of predicting the equilibrium curve in known as path-following (among the engineers) or continuation methods (among the mathematicians). The direct consequence of adding one more equation in the non-linear system is that existing solvers need to be adapted, which can be inconvenient in numerous situations. Later, Crisfield [24,25] showed that it would be possible to use existing solvers without any modification, provided that the corrections were obtained from two parts. A first part comes from the unbalance residue and a second results from applying a unit load standard in the same direction of the indirectly controlled load. These studies allowed essential advances for the Non-Linear Structural Analysis field, using the Finite Element Method in particular [26-28]. Over the last few years, only a few works studied the association of BEM with path-following techniques. Most path-following boundary element-based studies found in the literature, i.e., [29-32] for geometrically nonlinear bending problems and [33-37] for physically nonlinear problems induced by cracks, adopted Riks-like formulation combined with the so-called arc-length method. Although usual, this is not the only possible choice [22]. A unique path-equation that works well for all snapping cases is not known and it is up to the analyst to choose the most appropriated one for the case under study. There are basically two groups of path-following boundary element-based studies: (i) those that incorporate the path-equation into the equilibrium equation before proceeding the linearisation and (ii) those that use the path-following equations separately to calculate the load factor corrections, without including it in the equilibrium linearization. The last alternative is named partitioned approach.

Following the ideas presented by Oliveira *et al* [22] for a sub-region cohesive boundary element formulation, the present work proposes an alternative approach to introduce the cohesive models into the dual BEM formulation based on local cohesive stiffness matrices, which results in a residue that is written in terms of matrices that do not change dimension during the propagation process. Besides, a partitioned path-following technique with the direct control of one of the unknown degrees of freedom as the path-following equation is deduced to solve the resulting nonlinear problem. A simple numerical example is presented to validate the proposed approach.

2 Dual boundary element method

The dual boundary element method (dual BEM) is a widely used method for solving linear elastostatic problems containing crack. The method is based on the use of the dual Boundary Integral Equations (BIE´s) of linear elasticity [38]. In the following, the numerical solution of the dual BIE by a weighted residue collocation dual BEM is presented.

2.1 Boundary integral equations of linear elasticity

Consider an elastic cracked solid with domain $\mathbf{\Omega}$, external boundary $\mathbf{\Gamma}_\mathrm{b}$, internal crack boundary $\mathbf{\Gamma}_\mathrm{c}=\mathbf{\Gamma}_\mathrm{c}^+ \cup \mathbf{\Gamma}_\mathrm{c}^-$. The mechanical response of the solid can be represented in terms of the BIE's. The displacement (singular) BIE, assuming the body and inertia forces as nil, is written for a boundary source point $\mathbf{y}$ as follows

$$c_{ij}(\mathbf{y})u_j(\mathbf{y}) = \int_{\mathbf{\Gamma}} \mathrm{U}_{ij}(\mathbf{y},\mathbf{x})t_j(\mathbf{x})\,\mathrm{d}\mathbf{\Gamma} - \mathcal{C}\int_{\mathbf{\Gamma}} \mathrm{T}_{ij}(\mathbf{y},\mathbf{x})u_j(\mathbf{x})\,\mathrm{d}\mathbf{\Gamma} \tag{1}$$

where $\mathbf{y}$ and $\mathbf{x}$ indicates the source and field points, respectively. $u_j(\mathbf{y})$ is the displacement at $\mathbf{y}$. $u_j(\mathbf{x})$ and $t_j(\mathbf{x})$ are boundary displacements and tractions fields and, $\mathrm{U}_{ij}(\mathbf{y},\mathbf{x})$, $\mathrm{T}_{ij}(\mathbf{y},\mathbf{x})$ are, respectively, the Kelvin fundamental solutions for displacements and tractions, which are functions of the distance $r = \|\mathbf{r}\| = \|\mathbf{x}-\mathbf{y}\|$ [39 = Aliabadi, 2002]. $\mathcal{C}\int$ indicates that the integral is evaluated in the *Cauchy* Principal Value sense and $c_{ij}(\mathbf{y})u_j(\mathbf{y})$ is the free term arising from the singular integral. For a source point $\mathbf{y}^+$ at the crack face $\mathbf{\Gamma}_\mathrm{c}^+$, the displacement BIE reads

$$c_{ij}(\mathbf{y}^+)u_j(\mathbf{y}^+) + c_{ij}(\mathbf{y}^-)u_j(\mathbf{y}^-) = \int_{\mathbf{\Gamma}} \mathrm{U}_{ij}(\mathbf{y}^+,\mathbf{x})t_j(\mathbf{x})\,\mathrm{d}\mathbf{\Gamma} - \mathcal{C}\int_{\mathbf{\Gamma}} \mathrm{T}_{ij}(\mathbf{y}^+,\mathbf{x})u_j(\mathbf{x})\,\mathrm{d}\mathbf{\Gamma} \tag{2}$$

in which the additional free term $c_{\mathrm{ij}}(\mathbf{y}^-)\mathrm{u_j}(\mathbf{y}^-)$ appears due to the fact that $\mathbf{y}^-$ also lies on $\mathbf{\Gamma}_\mathrm{c}^+$. The traction (hyper-singular) BIE is obtained by the differentiation of the displacement BIE (1) with respect to $\mathbf{y}$, applying the constitutive relation (Hooke's law) and further the Cauchy formula for surface balance. The traction BIE written for a crack source point $\mathbf{y}^-$ at the crack face $\mathbf{\Gamma}_\mathrm{c}^-$ reads

$$\frac{1}{2}t_i(\mathbf{y}^-) - \frac{1}{2}t_i(\mathbf{y}^+) = \eta_j(\mathbf{y}^-)\mathcal{C}\int_{\mathbf{\Gamma}} \mathrm{D}_{kij}(\mathbf{y}^-,\mathbf{x})t_k(\mathbf{x})\,\mathrm{d}\mathbf{\Gamma} - \eta_j(\mathbf{y}^-)\mathcal{H}\int_{\mathbf{\Gamma}} \mathrm{S}_{kij}(\mathbf{y}^-,\mathbf{x})u_k(\mathbf{x})\,\mathrm{d}\mathbf{\Gamma} \tag{3}$$

where:

$$\mathrm{S}_{kij}(\mathbf{y}^-,\mathbf{x}) = \mathbb{C}_{kijl}\frac{\partial \mathrm{T}_{lm}(\mathbf{y}^-,\mathbf{x})}{\partial y_m^-} \qquad \mathrm{D}_{kij}(\mathbf{y}^-,\mathbf{x}) = \mathbb{C}_{kijl}\frac{\partial \mathrm{U}_{lm}(\mathbf{y}^-,\mathbf{x})}{\partial y_m^-} \tag{4}$$

$\mathbb{C}_{kijl}$ standing for the constitutive elastic components and $\mathcal{H}\int$ denotes a *Hadamard* Finite Part integral, which can only be defined for source points $\mathbf{y}^-$ lying on smooth boundaries. Thus, $c_{ij}(\mathbf{y}^+) = \delta_{ij}/2$ was considering in the deduction of (3).

2.2 Boundary approximations

Approximations are required for obtaining numerical solutions of the previous presented BIE´s by classical weighted residue collocation method. Thus, the boundaries $\mathbf{\Gamma}_\mathrm{b}$, $\mathbf{\Gamma}_\mathrm{c}^+$ and $\mathbf{\Gamma}_\mathrm{c}^-$ must be discretized into boundary elements, over which displacements, tractions, and the boundary geometry are approximated. Thus, Eq.´s (2-4) results

$$c_{ij}(\mathbf{y})u_j(\mathbf{y}) + \sum_{\mathrm{e}=1}^{\mathrm{NE}}\int_{\mathbf{\Gamma}_\mathrm{e}} \mathrm{T}_{ij}\big(\mathbf{y},\mathbf{x}(\xi)\big)N^\alpha(\xi)J(\xi)d\xi u_j^\alpha = \sum_{\mathrm{e}=1}^{\mathrm{NE}}\int_{\Gamma_\mathrm{e}} \mathrm{U}_{ij}\big(\mathbf{y},\mathbf{x}(\xi)\big)N^\alpha(\xi)J(\xi)d\xi t_j^\alpha \tag{5}$$

$$c_{ij}(\mathbf{y}^+)u_j(\mathbf{y}^+) + c_{ij}(\mathbf{y}^-)u_j(\mathbf{y}^-) + \sum_{\mathrm{e}=1}^{\mathrm{NE}}\int_{\mathbf{\Gamma}_\mathrm{e}} \mathrm{T}_{ij}\big(\mathbf{y}^+,\mathbf{x}(\xi)\big)N^\alpha(\xi)J(\xi)d\xi u_j^\alpha = \sum_{\mathrm{e}=1}^{\mathrm{NE}}\int_{\Gamma_\mathrm{e}} \mathrm{U}_{ij}\big(\mathbf{y}^+,\mathbf{x}(\xi)\big)N^\alpha(\xi)J(\xi)d\xi t_j^\alpha \tag{6}$$

$$\frac{1}{2}t_i(\mathbf{y}^-) - \frac{1}{2}t_i(\mathbf{y}^+) + \eta_j(\mathbf{y}^-)\sum_{e=1}^{NE}\int_{\Gamma_e} S_{kij}(\mathbf{y}^-,\mathbf{x}(\xi))N^\alpha(\xi)J(\xi)d\xi u_k^\alpha = \eta_j(\mathbf{y}^-)\sum_{e=1}^{NE}\int_{\Gamma_e} D_{kij}(\mathbf{y}^-,\mathbf{x}(\xi))N^\alpha(\xi)J(\xi)d\xi t_k^\alpha \quad (7)$$

where NE indicates the number of boundary elements utilized for discretizing the boundary $\boldsymbol{\Gamma} = \boldsymbol{\Gamma}_b \cup \boldsymbol{\Gamma}_c^+ \cup \boldsymbol{\Gamma}_c^-$, $\boldsymbol{\Gamma}_e$ represents the parametric curve or surface of a given element e, $N^\alpha(\xi)$ are basis functions (Lagrange polynomials are adopted in the present work), $J(\xi)$ is the Jacobian of the gaussian to physical space mapping and u_j^α and t_j^α are the displacements and tractions components at the collocation points (set equal to the source points), respectively. The singular and hypersingular integrals in (5), (6) and (7) are treated by the subtraction singularity technique [39] and the remaining regular integrals are performed with standard Gaussian quadrature. The BEM usual system of equations $\mathbf{Hu} = \mathbf{Gt}$ is thus obtained from the collocation of (5) for collocation points $\mathbf{y}$ lying on $\boldsymbol{\Gamma}_b$, (6) for collocation points $\mathbf{y}^+$ lying on $\boldsymbol{\Gamma}_c^+$ and (7) for collocation points $\mathbf{y}^-$ lying on $\boldsymbol{\Gamma}_c^-$. Discontinuous boundary elements, such as those presented in [39], are adopted in regions of geometric or traction discontinuities on and for the elements over the crack faces.

3 Cohesive dual boundary element method

A new dual boundary element formulation, capable of naturally introduce any desired cohesive behaviour for the tractions at the crack surfaces is presented. For illustration purposes, a very simple cohesive model is introduced into the dual BEM equations and the resulting nonlinear system is solved by a partitioned path following incremental-iterative approach, in which the magnitude (or load factor) of the acting forces is determined with respect to the equilibrium of the boundary fields (indirectly controlled) and an additional path-following constraint equation. Any unknown degree of freedom, i.e., boundary displacement and tractions, displacement of one face of the crack or the displacement discontinuities at the crack, can be chosen to be controlled.

3.1 A simple cohesive zone model

The normal and tangential cohesive tractions t_n and t_t, can be generally related to the normal and tangential displacement discontinuities, Δu_n and Δu_t, by cohesive stiffness k_n and k_t as follows:

$$\begin{Bmatrix} t_n \\ t_t \end{Bmatrix} = \begin{bmatrix} k_n(\Delta u_n, \Delta u_t) & \\ & k_t(\Delta u_n, \Delta u_t) \end{bmatrix} \begin{Bmatrix} \Delta u_n \\ \Delta u_t \end{Bmatrix} \quad (8)$$

which can be presented in matrix format as:

$$\bar{\mathbf{t}} = \bar{\mathbf{k}}(\Delta\bar{\mathbf{u}})\Delta\bar{\mathbf{u}} \quad (9)$$

In the present study, a simple cohesive model illustrated in Figure 2 is adopted.

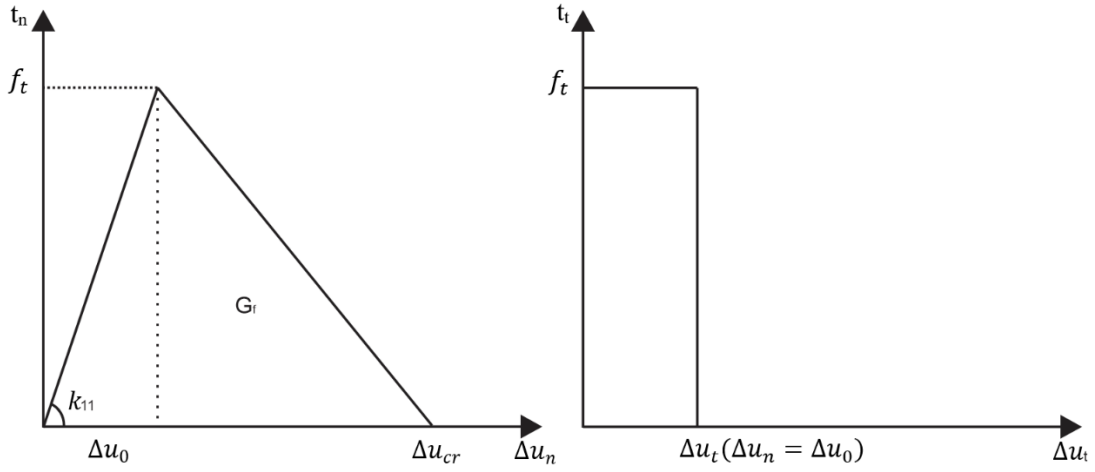

Figure 2. Cohesive zone model

The initial and critical normal displacement discontinuities are defined, respectively, as $\Delta u_0 = f_t/k_{n0}$ and $\Delta u_{cr} = 2G_f/f_t$. Where f_t is the material tensile strength, G_f the fracture energy and k_{n0}, k_{t0}, the initial cohesive stiffness in both normal and tangential diredawctions. For this simple model, the normal and tangential cohesive stiffness are given by:

$$k_n = \begin{cases} k_{n0} & 0 \le \Delta u_n \le \Delta u_0 \\ c\left(\dfrac{\Delta u_{cr}}{\Delta u_n} - 1\right) & \Delta u_0 \le \Delta u_n \le \Delta u_{cr} \\ 0 & \Delta u_n > \Delta u_{cr} \end{cases} \qquad k_t = \begin{cases} k_{t0} & 0 \le \Delta u_n \le \Delta u_0 \\ 0 & \Delta u_n > \Delta u_0 \end{cases} \tag{10}$$

where $c = f_t/(\Delta u_{cr} - \Delta u_0)$. Notice that, in this model, both k_n and k_t are exclusive functions of Δu_n. Besides, the definition of k_t in (10) implies a brittle shear behaviour to the model.
It is interesting to rewrite (9) in the global coordinate system for which the linear elasticity boundary value problem is defined. Thus, one defines a coordinate transformation $\mathbf{R}$ such that: t_n t_t

$$\bar{\mathbf{t}} = \bar{\mathbf{k}}(\Delta\bar{\mathbf{u}})\Delta\bar{\mathbf{u}} \quad \Rightarrow \quad \mathbf{R}^{\mathrm{T}}\mathbf{t} = \bar{\mathbf{k}}(\Delta\bar{\mathbf{u}})\mathbf{R}^{\mathrm{T}}\Delta\mathbf{u} \quad \Rightarrow \quad \mathbf{t} = \mathbf{R}\bar{\mathbf{k}}(\Delta\bar{\mathbf{u}})\mathbf{R}^{\mathrm{T}}\Delta\mathbf{u} \tag{11}$$

in which

$$\mathbf{R} = \begin{bmatrix} n_1 & t_1 \\ n_2 & t_2 \end{bmatrix} \quad \text{or} \quad \mathbf{R} = \begin{bmatrix} n_1 & -n_2 \\ n_2 & n_1 \end{bmatrix} \quad \text{with} \quad \mathbf{R}\mathbf{R}^{\mathrm{T}} = \mathbf{I} = \begin{bmatrix} 1 & 0 \\ 0 & 1 \end{bmatrix} \tag{12}$$

is the coordinate rotation transformation and $n_i = \boldsymbol{n}.\boldsymbol{e}_i$, are the cosines between the crack normal direction $\boldsymbol{n}$ and the basis vectors $\boldsymbol{e}_i$. Thus, in the global coordinate system, the cohesive model can be expressed as:

$$\mathbf{t} = \mathbf{k}(\Delta\bar{\mathbf{u}})\Delta\mathbf{u} \tag{13}$$

where:

$$\mathbf{k} = \mathbf{R}\bar{\mathbf{k}}\mathbf{R}^{t} = \begin{bmatrix} k_{11} & k_{12} \\ k_{21} & k_{22} \end{bmatrix} = \begin{bmatrix} n_1^2\mathrm{k}_n + n_2^2\mathrm{k}_t & n_1n_2\mathrm{k}_n - n_1n_2\mathrm{k}_t \\ n_1n_2\mathrm{k}_n - n_1n_2\mathrm{k}_t & n_2^2\mathrm{k}_n + n_1^2\mathrm{k}_t \end{bmatrix} \tag{14}$$

is the cohesive stiffnesses matrix, written for the global coordinate system.

3.2 Nonlinear system of equations

From Figure 1, it is possible to split the BEM linear system of equations governing regarding the classification of the collocation points belonging to the boundaries where displacement and tractions are prescribed and the positive and negative sides of the crack, where the cohesive model previously presented will be imposed. Thus:

$$\lambda\mathbf{H}_{\mathrm{u}}\bar{\mathbf{u}} + \mathbf{H}_{\mathrm{t}}\mathbf{u}_{\mathrm{t}} + \mathbf{H}_{\mathrm{c}}^{+}\mathbf{u}^{+} + \mathbf{H}_{\mathrm{c}}^{-}\mathbf{u}^{-} = \mathbf{G}_{\mathrm{u}}\mathbf{t}_{\mathrm{u}} + \lambda\mathbf{G}_{\mathrm{t}}\bar{\mathbf{t}} + \mathbf{G}_{\mathrm{c}}^{+}\mathbf{t}^{+} + \mathbf{G}_{\mathrm{c}}^{-}\mathbf{t}^{-} \tag{15}$$

from the prescribed boundary quantities $\bar{\mathbf{u}}$ and $\bar{\mathbf{t}}$, one computes the vectors: $\bar{\mathbf{F}}_{\mathrm{u}} = \mathbf{H}_u\bar{\mathbf{u}}$ and $\bar{\mathbf{F}}_{\mathrm{t}} = \mathbf{G}_t\bar{\mathbf{t}}$. Defining the displacement discontinuity vector $\Delta\mathbf{U} = \mathbf{u}^{+} - \mathbf{u}^{-}$ and imposing equilibrium of forces $\mathbf{t}^{+} + \mathbf{t}^{-} = \mathbf{0}$ at the crack surfaces, it is possible to rewrite (15) as:

$$\mathbf{H}_{\mathrm{t}}\mathbf{u}_{\mathrm{t}} - \mathbf{G}_{\mathrm{u}}\mathbf{t}_{\mathrm{u}} + [\mathbf{H}^{+} + \mathbf{H}^{-}]\mathbf{u}^{-} + \mathbf{H}^{+}\Delta\mathbf{U} = \lambda(\bar{\mathbf{F}}_{\mathrm{t}} - \bar{\mathbf{F}}_{\mathrm{u}}) + [\mathbf{G}^{+} - \mathbf{G}^{-}]\mathbf{t}^{+} \tag{16}$$

the cohesive model (14) can be introduced for governing the tractions $\mathbf{t}^{+}$: $\mathbf{t}^{+} = \mathbf{K}(\Delta\mathbf{U})\Delta\mathbf{U}$, resulting in:

$$\mathbf{H}_{\mathrm{t}}\mathbf{u}_{\mathrm{t}} - \mathbf{G}_{\mathrm{u}}\mathbf{t}_{\mathrm{u}} + [\mathbf{H}^{+} + \mathbf{H}^{-}]\mathbf{u}^{-} + [\mathbf{H}^{+} - [\mathbf{G}^{+} - \mathbf{G}^{-}]\mathbf{K}(\Delta\mathbf{U})]\Delta\mathbf{U} = \lambda(\bar{\mathbf{F}}_{\mathrm{t}} - \bar{\mathbf{F}}_{\mathrm{u}}) \tag{17}$$

where the matrix $\mathbf{K}$ collects the cohesive stiffness for all $N_{\Delta\boldsymbol{u}}$ pairs of coincident collocation points at the crack surface:

$$\mathbf{K}(\Delta\mathbf{U}) = \begin{bmatrix} k_{11}^{1} & k_{12}^{1} & k_{11}^{2} & k_{12}^{2} & \cdots & k_{11}^{N_{\Delta\boldsymbol{u}}} & k_{12}^{N_{\Delta\boldsymbol{u}}} \\ k_{21}^{1} & k_{22}^{1} & k_{21}^{2} & k_{22}^{2} & \cdots & k_{21}^{N_{\Delta\boldsymbol{u}}} & k_{22}^{N_{\Delta\boldsymbol{u}}} \end{bmatrix} \tag{18}$$

The nonlinear system of equations defined in (17) can be rewritten in matrix format as:

$$\mathbf{M}(\Delta\mathbf{U})\mathbf{X} = \lambda(\bar{\mathbf{F}}_{\mathrm{t}} - \bar{\mathbf{F}}_{\mathrm{u}}) \tag{19}$$

in which the matrix $\mathbf{M}$ and the vector of unknowns $\mathbf{X}$ are defined as:

$$\mathbf{M}(\Delta\mathbf{U}) = \left[\mathbf{H}_{\mathrm{t}} \quad -\mathbf{G}_{\mathrm{u}} \quad \mathbf{H}^{\pm} \quad \left(\mathbf{H}^{+} + \mathbf{G}^{\mp}\mathbf{K}(\Delta\mathbf{U})\right)\right] \qquad \mathbf{H}^{\pm} = [\mathbf{H}^{+} + \mathbf{H}^{-}] \qquad \mathbf{G}^{\mp} = [\mathbf{G}^{-} - \mathbf{G}^{+}] \tag{20}$$

$$\mathbf{X} = \begin{Bmatrix} \mathbf{u}_{\mathrm{t}} \\ \mathbf{t}_{\mathrm{u}} \\ \mathbf{u}^{-} \\ \Delta\mathbf{U} \end{Bmatrix} \tag{21}$$

For a non-equilibrated state of unknowns $(\mathbf{X}, \lambda)$,the residue vector can be defined as:

$$\mathbf{R}(\mathbf{X}, \lambda) = \mathbf{M}(\Delta\mathbf{U})\mathbf{X} - \lambda(\bar{\mathbf{F}}_{\mathrm{t}} - \bar{\mathbf{F}}_{\mathrm{u}}) \tag{22}$$

The definition of the residue vector is the starting point for the development of the consistent linearization presented in the following.

3.3 Consistent linearization and path-following constraint equation

In order to perform a consistent linearization, the Taylor expansion of the residual is required:

$$\mathbf{R}(\mathbf{X},\lambda) = \mathbf{R}(\mathbf{X_0},\lambda_0) + \left.\frac{\partial\mathbf{R}}{\partial\mathbf{X}}\right|_{\substack{\mathbf{X}=\mathbf{X_0}\\ \lambda=\lambda_0}} \Delta\mathbf{X} + \left.\frac{\partial\mathbf{R}}{\partial\lambda}\right|_{\substack{\mathbf{X}=\mathbf{X_0}\\ \lambda=\lambda_0}} \Delta\lambda + \theta(\Delta\mathbf{X}, \Delta\lambda) \tag{23}$$

Considering that $\Delta\mathbf{X}$ can be splited into prediction, $\Delta\mathbf{X}_{\boldsymbol{p}}$, and a correction, $\Delta\mathbf{X}_{\boldsymbol{c}}$, parts: $\Delta\mathbf{X} = \Delta\mathbf{X}_c + \Delta\lambda\Delta\mathbf{X}_p$, it is possible to enforce the equilibrium approximating (23) just with the linear term and enforcing $\mathbf{R}(\mathbf{X},\lambda) = \mathbf{0}$:

$$\mathbf{R}(\mathbf{X_0},\lambda_0) + \left.\frac{\partial\mathbf{R}}{\partial\mathbf{X}}\right|_{\substack{\mathbf{X}=\mathbf{X_0}\\ \lambda=\lambda_0}} \Delta\mathbf{X_c} + \left[\left.\frac{\partial\mathbf{R}}{\partial\mathbf{X}}\right|_{\substack{\mathbf{X}=\mathbf{X_0}\\ \lambda=\lambda_0}} \Delta\mathbf{X_p} + \left.\frac{\partial\mathbf{R}}{\partial\lambda}\right|_{\substack{\mathbf{X}=\mathbf{X_0}\\ \lambda=\lambda_0}}\right]\Delta\lambda = \mathbf{0} \tag{24}$$

Since $\Delta\lambda$ is an independent degree of freedom:

$$\left.\frac{\partial\mathbf{R}}{\partial\mathbf{X}}\right|_{\substack{\mathbf{X}=\mathbf{X_0}\\ \lambda=\lambda_0}} \Delta\mathbf{X_c} + \mathbf{R}(\mathbf{X_0},\lambda_0) = \mathbf{0} \tag{25}$$

$$\left.\frac{\partial\mathbf{R}}{\partial\mathbf{X}}\right|_{\substack{\mathbf{X}=\mathbf{X_0}\\ \lambda=\lambda_0}} \Delta\mathbf{X_p} + \left.\frac{\partial\mathbf{R}}{\partial\lambda}\right|_{\substack{\mathbf{X}=\mathbf{X_0}\\ \lambda=\lambda_0}} = \mathbf{0} \tag{26}$$

From (25) and (26) it is possible to obtain $\Delta\mathbf{X_c}$ and $\Delta\mathbf{X_p}$. An additional constraint equation is required to determine $\Delta\lambda$. The chosen equation is the direct control of one direction $\boldsymbol{e}_i$ of $\mathbf{X}$. Thus:

$$\boldsymbol{e}_i.\mathbf{X} = \bar{\mathrm{X}} \qquad \Rightarrow \qquad \boldsymbol{e}_i.\boldsymbol{\Delta}\mathbf{X} = 0 \qquad \Rightarrow \qquad \Delta\lambda = -\frac{\boldsymbol{e}_i.\boldsymbol{\Delta}\mathbf{X}_c}{\boldsymbol{e}_i.\boldsymbol{\Delta}\mathbf{X}_p} \tag{27}$$

From $\Delta\mathbf{X}_{\mathrm{c}}$, $\Delta\mathbf{X}_{\mathrm{p}}$ and $\Delta\lambda$ it is possible to obtain the improved solution:

$$\boldsymbol{\Delta}\mathbf{X} = \Delta\mathbf{X}_{\mathrm{c}} + \Delta\lambda\Delta\mathbf{X}_{\mathrm{p}}$$

$$\mathbf{X} = \mathbf{X}_0 + \boldsymbol{\Delta}\mathbf{X}$$

$$\lambda = \lambda_0 + \Delta\lambda \tag{28}$$

which must be used as a new guest for the equilibrium solution, i.e., $\mathbf{X}_0 = \mathbf{X}$ and $\lambda_0 = \lambda$, until the residue vector

is close enough to be null, according to a convergence criterion. The vector $\partial\mathbf{R}/\partial\lambda$ results $\bar{\mathbf{F}}_{\mathrm{t}} - \bar{\mathbf{F}}_{\mathrm{u}}$. On the other hand, the tangent matrix $\partial\mathbf{R}/\partial\mathbf{X}$ is derived in the following.

3.4 Tangent matrix

The residue can be previously presented in (22) can expressed as:

$$\mathbf{R}(\mathbf{X},\lambda) = \begin{bmatrix}\mathbf{H}_{\mathrm{t}} & -\mathbf{G}_{\mathrm{u}} & \mathbf{H}^{\pm} & \left(\mathbf{H}^{+} + \mathbf{G}^{\mp}\mathbf{K}(\Delta\mathbf{U})\right)\end{bmatrix}\begin{Bmatrix}\mathbf{u}_{\mathrm{t}}\\ \mathbf{t}_{\mathrm{u}}\\ \mathbf{u}^{-}\\ \Delta\mathbf{U}\end{Bmatrix} - \lambda(\bar{\mathbf{F}}_{\mathrm{t}} - \bar{\mathbf{F}}_{\mathrm{u}}) \tag{29}$$

$$\mathbf{R}(\mathbf{X},\lambda) = \mathbf{F}_{\mathrm{u}} + \mathbf{F}_{\mathrm{t}} + \mathbf{F}_{\mathrm{u}^{-}} + \mathbf{F}_{\Delta\mathrm{u}} - \lambda(\bar{\mathbf{F}}_{\mathrm{t}} - \bar{\mathbf{F}}_{\mathrm{u}})$$

From (29), the tangent matrix results:

$$\frac{\partial\mathbf{R}}{\partial\mathbf{X}} = \begin{bmatrix}\dfrac{\partial\mathbf{R}}{\partial\mathbf{u}} & \dfrac{\partial\mathbf{R}}{\partial\mathbf{t}} & \dfrac{\partial\mathbf{R}}{\partial\mathbf{u}^{-}} & \dfrac{\partial\mathbf{R}}{\partial\Delta\mathbf{U}}\end{bmatrix} \tag{30}$$

in which:

$$\frac{\partial\mathbf{R}}{\partial\mathbf{u}} = \frac{\partial\mathbf{F}_{\mathrm{u}}}{\partial\mathbf{u}} = \mathbf{H}_{\mathrm{t}} \qquad \frac{\partial\mathbf{R}}{\partial\mathbf{t}} = \frac{\partial\mathbf{F}_{\mathrm{t}}}{\partial\mathbf{u}} = -\mathbf{G}_{\mathrm{u}}$$

$$\frac{\partial\mathbf{R}}{\partial\mathbf{u}^{-}} = \frac{\partial\mathbf{F}_{\mathrm{u}^{-}}}{\partial\mathbf{u}^{-}} = \mathbf{H}^{\pm} \qquad \frac{\partial\mathbf{R}}{\partial\Delta\mathbf{U}} = \frac{\partial\mathbf{F}_{\Delta\mathbf{U}}}{\partial\Delta\mathbf{U}} = \mathbf{H}^{+} + \frac{\partial\left(\mathbf{G}^{\mp}\mathbf{K}\Delta\mathbf{U}\right)}{\partial\Delta\mathbf{U}} \tag{31}$$

The last derivative in (31) can be computed as:

$$\frac{\partial\left(\mathbf{G}^{\mp}\mathbf{K}(\Delta\mathbf{U})\Delta\mathbf{U}\right)}{\partial\Delta\mathbf{U}} = \mathbf{G}^{\mp}\mathbf{K} + \mathbf{G}^{\mp}\frac{\partial(\mathbf{K}\Delta\mathbf{U}_{c})}{\partial\Delta\mathbf{U}} \tag{32}$$

The subscript "c" in $\Delta\mathbf{U}_{c}$ indicates that the derivative is performed keeping $\Delta\mathbf{U}_{c}$ constant:

$$\frac{\partial(\mathbf{K}\Delta\mathbf{U}_{c})}{\partial\Delta\mathbf{U}} = \sum_{i=1}^{N_{\Delta\boldsymbol{u}}}\left(\Delta u_{2i-1}\frac{\partial\mathbf{K}_{2i-1}}{\partial\Delta\mathbf{U}} + \Delta u_{2i}\frac{\partial\mathbf{K}_{2i}}{\partial\Delta\mathbf{U}}\right) \tag{33}$$

where Δu_{2i-1} and Δu_{2i} are the odd and even components of $\Delta\mathbf{U}$, respectively. Analogously, $\mathbf{K}_{2i-1}$ and $\mathbf{K}_{2i}$ are the odd and even columns of $\mathbf{K}$.

$$\mathbf{K}_{2i-1} = \begin{Bmatrix}k_{11}^{i}\\ k_{21}^{i}\end{Bmatrix} \qquad \mathbf{K}_{2i} = \begin{Bmatrix}k_{12}^{i}\\ k_{22}^{i}\end{Bmatrix} \tag{34}$$

The derivatives in (34) reads:

$$\frac{\partial\mathbf{K}_{2i-1}}{\partial\Delta\mathbf{U}} = \begin{bmatrix}\dfrac{\partial\mathbf{K}_{2i-1}}{\partial\Delta\boldsymbol{u}^{1}} & \cdots & \dfrac{\partial\mathbf{K}_{2i-1}}{\partial\Delta\boldsymbol{u}^{N_{\Delta u}}}\end{bmatrix} \qquad \frac{\partial\mathbf{K}_{2i}}{\partial\Delta\mathbf{U}} = \begin{bmatrix}\dfrac{\partial\mathbf{K}_{2i}}{\partial\Delta\boldsymbol{u}^{1}} & \cdots & \dfrac{\partial\mathbf{K}_{2i}}{\partial\Delta\boldsymbol{u}^{N_{\Delta u}}}\end{bmatrix} \tag{35}$$

where:

$$\frac{\partial\mathbf{K}_{2i-1}}{\partial\Delta\boldsymbol{u}^{j}} = \begin{bmatrix}\dfrac{\partial k_{11}^{i}}{\partial\Delta u_{x}^{j}} & \dfrac{\partial k_{11}^{i}}{\partial\Delta u_{y}^{j}}\\ \dfrac{\partial k_{21}^{i}}{\partial\Delta u_{x}^{j}} & \dfrac{\partial k_{21}^{i}}{\partial\Delta u_{y}^{j}}\end{bmatrix} \qquad \frac{\partial\mathbf{K}_{2i}}{\partial\Delta\boldsymbol{u}^{j}} = \begin{bmatrix}\dfrac{\partial k_{12}^{i}}{\partial\Delta u_{x}^{j}} & \dfrac{\partial k_{12}^{i}}{\partial\Delta u_{y}^{j}}\\ \dfrac{\partial k_{22}^{i}}{\partial\Delta u_{x}^{j}} & \dfrac{\partial k_{22}^{i}}{\partial\Delta u_{y}^{j}}\end{bmatrix} \tag{36}$$

Regarding the derivative change rule:

$$\frac{\partial k_{ij}}{\partial \Delta u_k} = \frac{\partial k_{ij}}{\partial \Delta u_n}\frac{\partial \Delta u_n}{\partial \Delta u_k} + \frac{\partial k_{ij}}{\partial \Delta u_t}\frac{\partial \Delta u_t}{\partial \Delta u_k} \tag{37}$$

in which de derivatives $\partial k_{ij}/\partial \Delta u_n$ and $\partial k_{ij}/\partial \Delta u_t = 0$ are computed from (14). From the transformation **R**, one also notices that $\partial \Delta u_n/\partial \Delta u_k = n_k$ and $\partial \Delta u_t/\partial \Delta u_k = t_k$. Thus, (36) can be rewritten for the adopted cohesive model in terms of its normal cohesive stiffness derivatives as:

$$\frac{\partial \mathbf{K}_{2i-1}}{\partial \Delta \boldsymbol{u}^j} = \begin{bmatrix} {n_1}^3 \dfrac{\partial k_n^i}{\partial \Delta u_n^j} & {n_1}^2 n_2 \dfrac{\partial k_n^i}{\partial \Delta u_n^j} \\ {n_1}^2 n_2 \dfrac{\partial k_n^i}{\partial \Delta u_n^j} & n_1 {n_2}^2 \dfrac{\partial k_n^i}{\partial \Delta u_n^j} \end{bmatrix} \qquad \frac{\partial \mathbf{K}_{2i}}{\partial \Delta \boldsymbol{u}^j} = \begin{bmatrix} {n_1}^2 n_2 \dfrac{\partial k_n^i}{\partial \Delta u_n^j} & n_1 {n_2}^2 \dfrac{\partial k_n^i}{\partial \Delta u_n^j} \\ n_1 {n_2}^2 \dfrac{\partial k_n^i}{\partial \Delta u_n^j} & {n_2}^3 \dfrac{\partial k_n^i}{\partial \Delta u_n^j} \end{bmatrix} \tag{38}$$

the cosines n_i in (37) are with respect to the $\boldsymbol{\Gamma}_c^+$ crack surface. Finally, the derivatives $\partial k_n^i/\partial \Delta u_n^j$ can be computed from (10) and results:

$$\frac{\partial k_n^i}{\partial \Delta u_n^j} = \begin{cases} 0 & \text{if } i \neq j \\ \dfrac{\partial k_n}{\partial \Delta u_n}(\Delta u_n^i) & \text{if } i = j \end{cases} \tag{39}$$

$$\frac{\partial k_n}{\partial \Delta u_n}(\Delta u_n^i) = \begin{cases} -c\dfrac{\Delta u_{cr}}{{\Delta u_n^i}^2} & \Delta u_0 \leq \Delta u_n^i \leq \Delta u_{cr} \\ 0 & \text{other wise} \end{cases} \tag{40}$$

4 Numerical results

A tensile sheet with a vertical cohesive crack, illustrated in Figure 3, was used as an example to test and validate the formulation. Three boundary element meshes m_1, m_2 and m_3, with 24, 48 and 96 elements, were adopted.

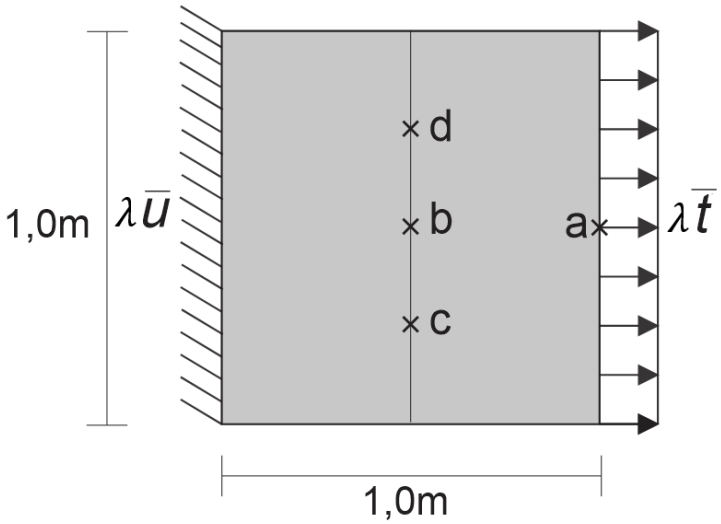

Figure 3-Tensile sheet: Geometry and boundary conditions

The adopted elastic constants were: E = 30 GPa and ν = 0.3. For the cohesive crack, the material parameters $k_{n0} = k_{t0} = 30E^7$GPa, $f_t = 3.0$ MPa and $G_f = 0.015$ MPa/m were adopted. A constant horizontal load patter is applied on the right side of the sheet in the form of an indirectly controlled load $\mathbf{t} = \lambda\bar{\mathbf{t}}$, in which $\bar{\mathbf{t}} = \{1 \quad 0\}^{\mathrm{T}}\mathrm{N/m}$ and λ is the load factor. The left side of the sheet was kept constrained, i.e., $\mathbf{u} = \lambda\bar{\mathbf{u}} = \mathbf{0}$. A plane stress condition and unit thickness are assumed for the sheet. The horizontal displacement $u_x = 0.0005$ m was imposed for the point "a" in 100 steps using the path-following incremental-iterative process with a convergence tolerance of 10^{-4}.

The force-displacement curves obtained for the three meshes are illustrated in Figure 4. The results shows that the structure bears force increments until it reaches a critical load, where the cohesive behaviour is activated, and the interface starts to open in mode I. The imposed displacement continues to increase, penalizing thus the cohesive stiffness (see Figure 5) until the end of the steps, when the structure will be deformed and all the points in the right side of the sheet dislocates approximately 0.0005 m in the x direction.

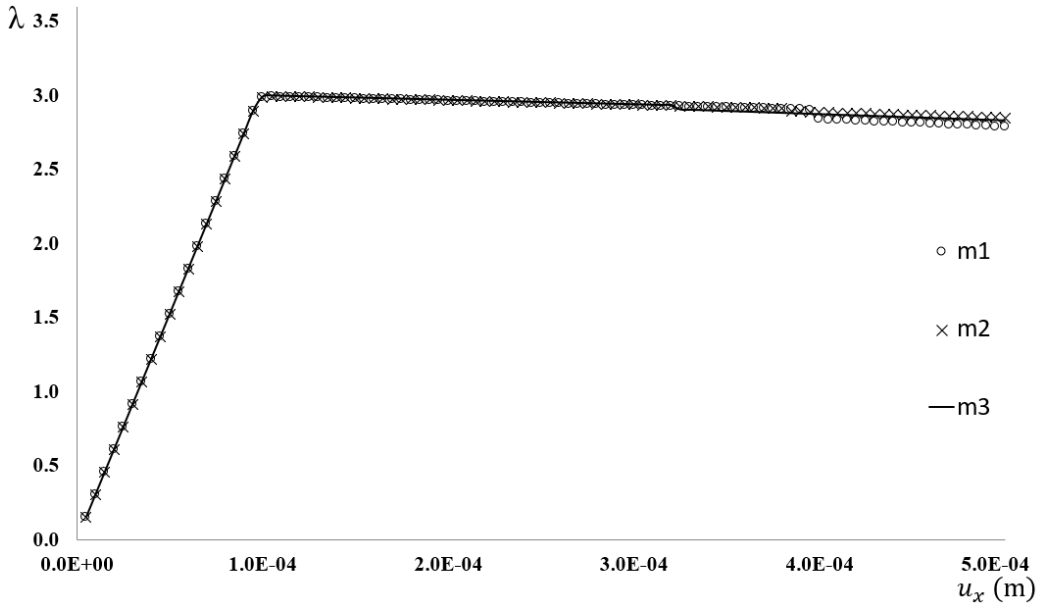

Figure 4- Structural response at point "a": λ versus u_x

Figure 5 illustrates the cohesive response for the point "b" at the interface. The results show that the cohesive behaviour described in Eq. (10) was successfully imposed for the interface nodes. Thus, when $\Delta u_n \leq \Delta u_0$, the normal and tangential tractions results $\mathrm{t}_n = k_{n0}\Delta u_n$, $\mathrm{t}_t = k_{t0}\Delta u_t$, and the structural behaviour is linear and very close to a non-cracked solid due to the high values adopted for k_{n0} and k_{t0}. After this, the cohesive behaviour starts until $\Delta u_n = \Delta u_{cr}$, when a perfect crack surface appears, i.e., $\mathrm{t}_n = \mathrm{t}_t = 0$.

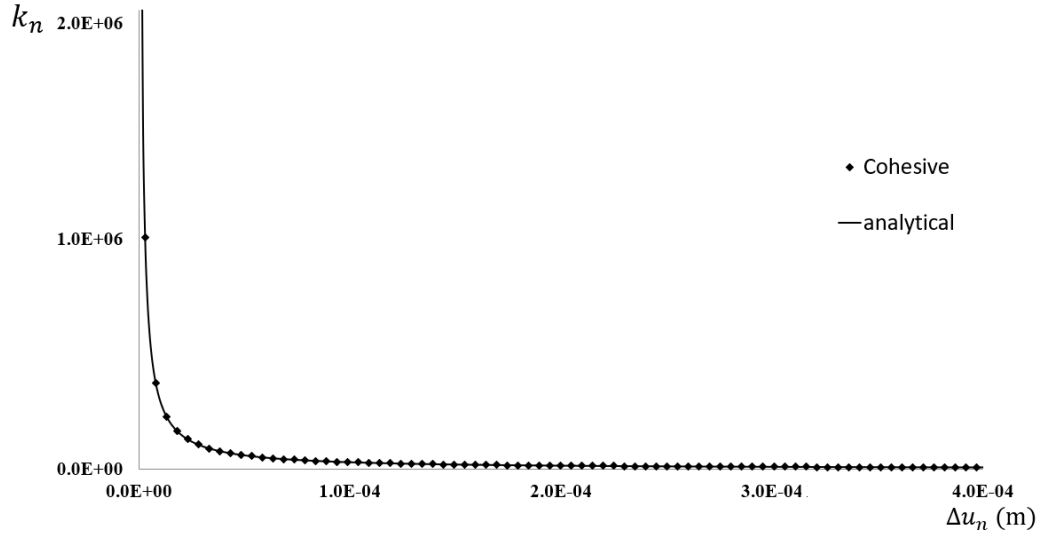

Figure 5- Cohesive response at point "b": K_n versus Δu_n

Figure 6 shows the response for the tangential displacement discontinuity Δu_t at points "c" and "d", symmetrically positioned along the crack with respect to the central point "b", with respect to the load factor λ. The smaller values of Δu_t compared to Δu_n and the symmetric response are in accordance with the expected mechanical response of this problem. Finally, for illustration purposes, Figure7 shows the displacements fields u_x, u_y and the principal stress fields σ_1, σ_2 for a distribution of 306 points (96 boundary points and 210 internal points), which are computed in a post-processing phase.

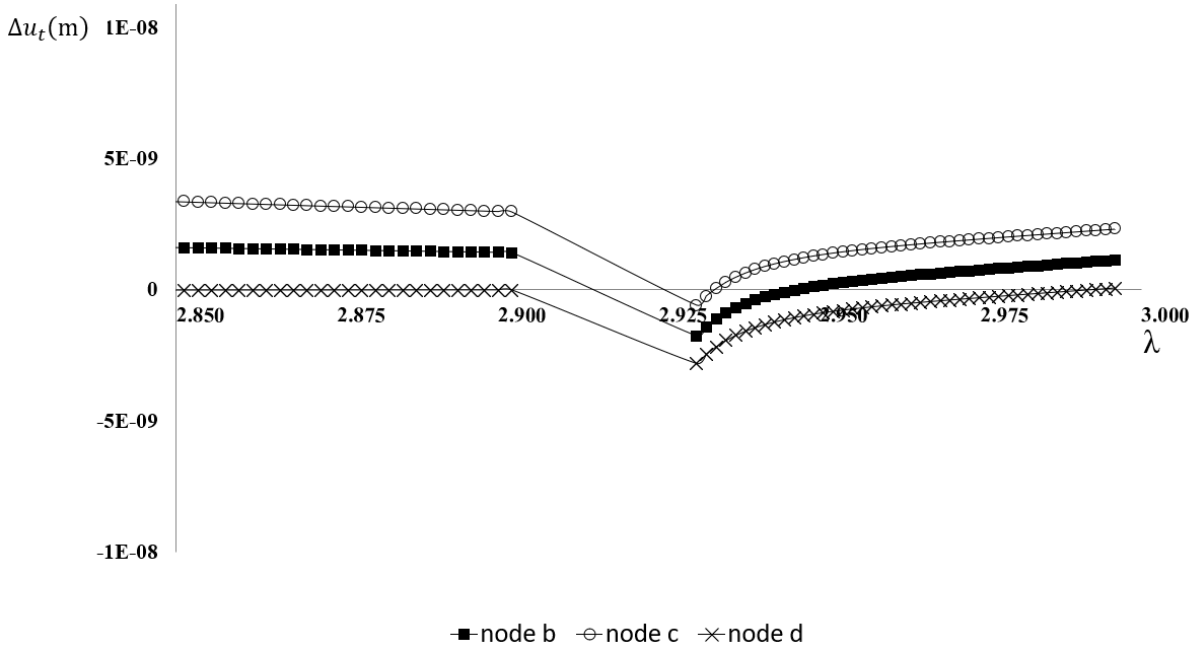

Figure 6- Brittle shear behaviour at points "b", "c" and "d": Δu_t versus λ

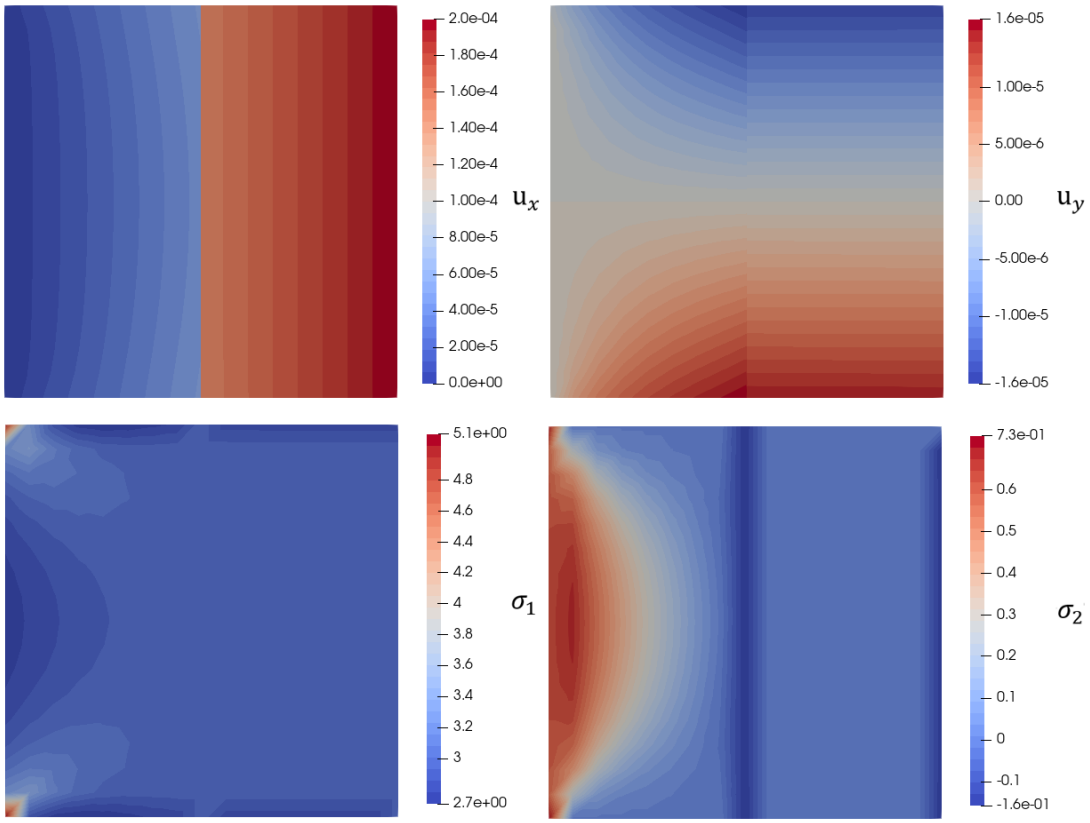

Figure 7- Numerical fields a) $u_x$displacement b) u_y displacement c) σ_1 principal stress d) σ_2 principal stress

5 Conclusions

A new cohesive dual boundary element formulation was developed for addressing crack propagation analysis. The main advantage of the formulations is that the cohesive law is introduced into the dual BEM equations by local cohesive stiffness, which degrades during the crack opening process. Within this framework, different cohesive laws, including damage-based ones for instance, could be easily account into the cohesive dual BEM. Besides, the dimensions of the dual BEM sub-matrices involved in the residue vector are kept constant throughout the hole crack propagation processes. A simple linear cohesive model is adopted to illustrate and validate the formulation. A path-following incremental iterative method with constraint equation that imposes the direct control of one direction of the unknown boundary values is adopted to solve the nonlinear system of equations. One example was presented to validate the formulation for cohesive crack propagation analysis. The results showed that the proposed approach can efficiently capture the equilibrium curves and the cohesive responses.

Acknowledgements. The authors would like to thank the financial support provided by the Coordination for the Improvement of Higher Education Personnel (CAPES).

Authorship statement. The authors hereby confirm that they are the sole liable persons responsible for the authorship of this work, and that all material that has been herein included as part of the present paper is either the property (and authorship) of the authors or has the permission of the owners to be included here.

References

[1] J. Lemaitre. *A Course on Damage Mechanics*. Springer Science & Business Media, 2013.
[2] C. Miehe, F. Welschinger, M. Hofacker, "Thermodynamically consistent phase-field models of fracture: Variational principles and multi-field FE implementations". *International Journal for Numerical Methods in Engineering*, vol. 83, n. 10, pp. 1273–1311, 2010.
[3] T. L. Anderson. *Fracture Mechanics: Fundamentals and Applications*. Boca Raton, 2017.
[4] K. Park and G. H. Paulino, "Cohesive Zone Models: A Critical Review of Traction-Separation Relationships Across Fracture Surfaces". *Applied Mechanics Reviews*, vol. 64, pp. 060802-1, 2011.
[5] D. S. Dugdale, "Yielding of steel sheets containing slits". *Journal of the Mechanics and Physics of Solids*, vol. 8, pp. 100-104, 1960.
[6] G. I. Barenblatt, "Mathematical theory of equilibrium cracks in brittle fracture". *Advances in Applied Mechanics*, vol. 7, pp. 55-129, 1962.
[7] K. L. Roe and T. Siegmund, "An irreversible cohesive zone model for interface fatigue crack growth simulation". *Engineering Fracture Mechanics*, vol. 70, pp. 209-232, 2003.
[8] H. K. Hong and J. T. Chen, "Derivations of integral equations of elasticity". *Journal of Engineering Mechanics*, vol. 114, pp. 1028-1044, 1988.
[9] H. K. Hong and J. T. Chen, "Generality and special cases of dual integral equations of elasticity". *Journal of the Chinese Society of Mechanical Engineers*, vol. 9, pp. 1-9, 1988.
[10] A. Portela, M. H. Aliabadi and D. P. Rooke, "The dual boundary element method: effective implementation for crack problems". *International journal for numerical methods in engineering*, vol. 33, n. 6, pp. 1269-1287, 1992.
[11] S. L. Grouch, "Solution of plane elasticity problems by the displacement discontinuity method". *International journal for numerical methods in engineering*, vol. 10, pp. 301-342, 1976.
[12] H. T. Xiao and Z. Q. Yue, "A Three-dimensional displacement discontinuity method for crack problems in layered rocks". *International Journal of Rock Mechanics and Mining Sciences*, vol. 48, pp. 412-420, 2011.
[13] G. E. Blandford, A. R. Ingraffea and J. A. Liggett, "Two-dimensional stress intensity factor computations using the boundary element method". *International Journal for Numerical Methods in Engineering*, vol. 17, n. 3, pp. 387-404, 1981.
[14] I. Benedetti and M. H. Aliabadi, "A three-dimensional cohesive-frictional grain-boundary micromechanical model for intergranular degradation and failure in polycystalline materials". *Computer Methods in Applied Mechanics and Engineering*, vol. 265, pp. 36-62, 2013.
[15] J. C. F. Telles and S. Guimarães, "Green´s function: a numerical generation for fracture mechanics problems via boundary elements". *Computer Methods in Applied Mechanics and Engineering*, vol. 188, pp. 847-858, 2000.

[16] W. S. Venturini, "A new boundary element formulation for crack analysis". *Transactions on Modelling and Simulation*, vol. 7, pp. 1-8, 1994.
[17] H. L. Oliveira and E. D. Leonel, "Cohesive crack growth modelling based on an alternative nonlinear BEM formulation". *Engineering Fracture Mechanics*, vol. 111, pp. 86-97, 2013.
[18] A. Frangi, G. Novati, R. Springhetti and M. Rovizzi, "3D fracture analysis by the symmetric Galerkin BEM". *Computational Mechanics*, vol. 28, pp. 220-232, 2002.
[19] A. L. Saleh, M. H. Aliabadi, "Crack growth analysis in concrete using boundary element method". *Engineering fracture mechanics*, vol. 51, n. 4, pp. 533-545, 1995.
[20] E. D. Leonel and W. S. Venturini, "Non-linear boundary element formulation with tangent operator to analyse crack propagation in quasi-brittle materials". *Engineering Analysis with Boundary Elements*, vol. 34, n. 2, pp. 122-129, 2010.
[21] S. G. F. Cordeiro and E. D. Leonel, "Cohesive crack propagation modelling in wood structures using BEM and the Tangent Operator Technique". *Engineering Analysis with Boundary Elements*, vol. 64, pp. 111-121, 2016.
[22] H. L. Oliveira, G. Rastiello and A. Millard, "Partitioned path-following strategy for nolinear structural analyses using the boundary element method". *Computer Methods in Applied Mechanics and Engineering*, vol. 394, pp. 114875, 2022.
[23] E. Riks, The application of newton's method to the problem of elastic stability, *Transactions of the ASME* (1972) 1060-1065.
[24] M. A. Crisfield, A fast incremental/iterative solution procedure that handles "snap-through", in: *Computational methods in nonlinear structural and solid mechanics*, Elsevier, 1981, pp. $55-62 .
[25] M. Crisfield, An arc-length method including line searches and accelerations, *International journal for numerical methods in engineering* 19 (9) (1983) 1269-1289 .
[26] E. Lorentz, P. Badel, A new path-following constraint for strain-softening finite element simulations, International journal for numerical methods in engineering 60 (2) (2004) 499-526.
[27] G. Rastiello, F. Riccardi, B. Richard, Discontinuity-scale path-following methods for the embedded discontinuity finite element modeling of failure in solids, *Computer Methods in Applied Mechanics and Engineering* 349 (2019) 431-457.
[28] H. L. Oliveira, G. Rastiello, A. Millard, I. Bitar, B. Richard, Modular implementation framework of partitioned pathfollowing strategies: Formulation, algorithms and application to the finite element software cast3m, *Advances in Engineering Software* 161 (2021) 103055. doi:https://doi.org/10.1016/j.advengsoft.2021.103055.
[29] N. Tosaka, S. Miyake, Geometrically nonlinear analysis of shallow spherical shell using an integral equation method, in: *Boundary Elements VIII*, Springer, 1986, pp. 537-546 .
[30] N. Tosaka, M. Nonaka, S. Miyake, Bifurcation analysis of elastic shallow arch by the boundary-domain element method, in: *Boundary Element Methods in Engineering*, Springer, 1990, pp. 286-292.
[31] M. Tanaka, T. Matsumoto, Z. Zheng, Application of the boundary-domain element method to the pre/post-buckling problem of von karman plates, *Engineering analysis with boundary elements* 23 (5-6) (1999) 399-404.
[32] O. Askour, S. Mesmoudi, A. Tri, B. Braikat, H. Zahrouni, M. Potier-Ferry, Method of fundamental solutions and a high order continuation for bifurcation analysis within föppl-von karman plate theory, *Engineering Analysis with Boundary Elements* 120 (2020) 67-72.
[33] A. Carpinteri, I. Monetto, Snap-back analysis of fracture evolution in multi-cracked solids using boundary element method, *International Journal of Fracture* 98 (3) (1999) 225-241.
[34] V. Mallardo, C. Alessandri, Arc-length procedures with bem in physically nonlinear problems, *Engineering analysis with boundary elements* 28 (6) (2004) 547-559 .
[35] V. Mallardo, Erratum to "arc-length procedures with bem in physically nonlinear problems"[*Engineering analysis with boundary elements* 28 (2004) 547-559], *Engineering Analysis with Boundary Elements* 8 (29) (2005) 828.
[36] L. A. Távara Mendoza, V. Mantic, L. Gray, F. París Carballo, A. Salvadori, Formulation and implementation of cohesive fracture models in the symmetric galerkin boundary element method. study of mode i crack growth, *Anales de Mecánica de la Fractura*, 2 (26), 435-440. (2009).
[37] F. Freddi, M. Savoia, Analysis of frp-concrete debonding via boundary integral equations, *Engineering Fracture Mechanics* 75 (6) (2008) 1666-1683.
[38] M. H. Aliabadi. The Boundary Element Method: *Applications in Solids and Structures*. Wiley, 2002.